Article

Prominent increases of nuclear DNAJA3 and cytosolic STAT1 with nucleic acid sensors underlie innate immunity activation in ClpP-null mouse

Antonia Maletzko [1#], Jana Key [1,2#], Ilka Wittig [3], Suzana Gispert [1], Gabriele Koepf [1], Júlia Canet-Pons [1], Sylvia Torres-Odio [1,4], A. Phillip West [4], Georg Auburger [1*]

[1] Experimental Neurology, Medical School, Goethe University, 60590 Frankfurt am Main, Germany; tmaletzko@online.de (A.M.); key@stud.uni-frankfurt.de (J.K.); Gispert-Sanchez@em.uni-frankfurt.de (S.G.); Gabriele.Koepf@kgu.de (G.K.); jcanetpons@gmail.com (J.C.-P.); sylviatorres494@gmail.com (S.T.-O.)
[2] Faculty of Biosciences, Goethe-University, Altenhöferallee 1, 60438 Frankfurt am Main, Germany;
[3] Functional Proteomics, Faculty of Medicine, Goethe University, 60590 Frankfurt am Main, Germany; Wittig@med.uni-frankfurt.de (I.W.)
[4] Department of Microbial Pathogenesis and Immunology, College of Medicine, Texas A&M, University Health Science Center, Bryan, TX 77807, USA; awest@medicine.tamhsc.edu (A.P.W.).
[#] Joint first authorship
• Correspondence: auburger@em.uni-frankfurt.de; Tel.: +49-(0)-69-6301-7428

Abstract: Mitochondrial dysfunctions, e.g. abnormal handling of mitochondrial DNA in TFAM mutants or in altered mitophagy, activate innate immunity. Recent reports also showed that deletion of mitochondrial matrix peptidase ClpP in mice transcriptionally upregulates inflammatory factors. Here, we studied ClpP-null mouse brain at two ages and embryonal fibroblasts, to identify which signaling pathways are responsible, employing mass spectrometry, immunoblots, and reverse transcriptase polymerase chain reaction. Anomalies in the mitochondrial unfolded protein responses pathway were prominent for the co-chaperone DNAJA3, and for its known interactor STAT1. Their mitochondrial dysregulation affected also their extra-mitochondrial abundance, as possible innate immune modulators. Increased expression was observed not only for the transcription factors *Stat1/2*, but also for two interferon-stimulated genes (*Ifi44*, *Gbp3*). Inflammatory responses were strongest for RLR pattern recognition receptors (*Ddx58*, *Ifih1*, *Oasl2*, *Trim25*) and several cytosolic nucleic acid sensors (*Ifit1*, *Ifit3*, *Oas1b*, *Ifi204*, *Mnda*). They can be explained by the accumulation of mitoribosomes and mitochondrial nucleoids in ClpP-null cells, which may act as damage-associated molecular patterns. The consistent dysregulation of these factors from early age might influence also human Perrault syndrome, where ClpP loss-of-function leads to early infertility and deafness, with subsequent widespread neurodegeneration.

Keywords: PRLTS3; Release of mtDNA and mtRNA; cGAS-STING; Leukodystrophy; Ataxia; mitochondrial amino acid tRNA synthetases; TWINKLE; POLG; MTRNR1.

1. Introduction

Mutations in the mitochondrial matrix peptidase ClpP in the human organism lead to Perrault syndrome type 3 (PRLTS3). This syndrome was initially described as autosomal recessive premature ovarian failure combined with sensorineural hearing loss, and was then shown to be accompanied by a growth deficit and a generalized neurodegenerative process with leukodystrophy upon neuroimaging, which manifests as late-onset progressive ataxia and neuropathy [1-5]. ClpP is highly conserved from bacteria to mammals, playing a crucial role for mitochondrial responses to unfolded protein stress (UPR^{mt}) by the disaggregases ClpX and ClpB, chaperones of the Hsp70 and Hsp60 family, as well as co-chaperones of the DnaJ and the GrpE family [6]. Thus, ClpP deficiency leads to problems for the assembly of proteins with RNA in mitoribosomes and with DNA in mitochondrial nucleoids [7-9]. This mitochondrial pathology triggers innate immunity activation in the eukaryotic

Preprints (www.preprints.org) | NOT PEER-REVIEWED | Posted: 4 May 2021 doi:10.20944/preprints202105.0021.v1

host cell to a degree where altered skin microbiome defenses can modify the lifespan of ClpP-null mice [10, 11], mainly via abnormal mtDNA that activates cGAS-STING signaling to modulate type I interferon release [9].

Other genetic causes of Perrault syndrome include mutations in the mitoribosome chaperone ERAL1, the mitochondrial amino acid tRNA transferases HARS2 and LARS2, and the mitochondrial translation factor RMND1, highlighting the importance of mitoribosomal translation for fertility and neurodegeneration. Additional causes are mutations in the mitochondrial DNA helicase-primase TWNK and the mitochondrial transcription factor TFAM, emphasizing the relevance of mtDNA disassembly. Perrault syndrome was also reported to be caused by mutations in the peroxisomal factors HSD17B4 and PEX6, or in GGPS1 as an enzyme responsible for prenylation of proteins, which is a determinant of UPR^{mt} [9, 12-14]. Also maternally inherited mutations in the mitochondrial DNA are known to cause progressive deafness via altered mitoribosome functions, and the chronic administration of aminoglycoside antibiotics can also lead to hearing deficits, presumably via their impact on mitoribosomal translation fidelity [15-17].

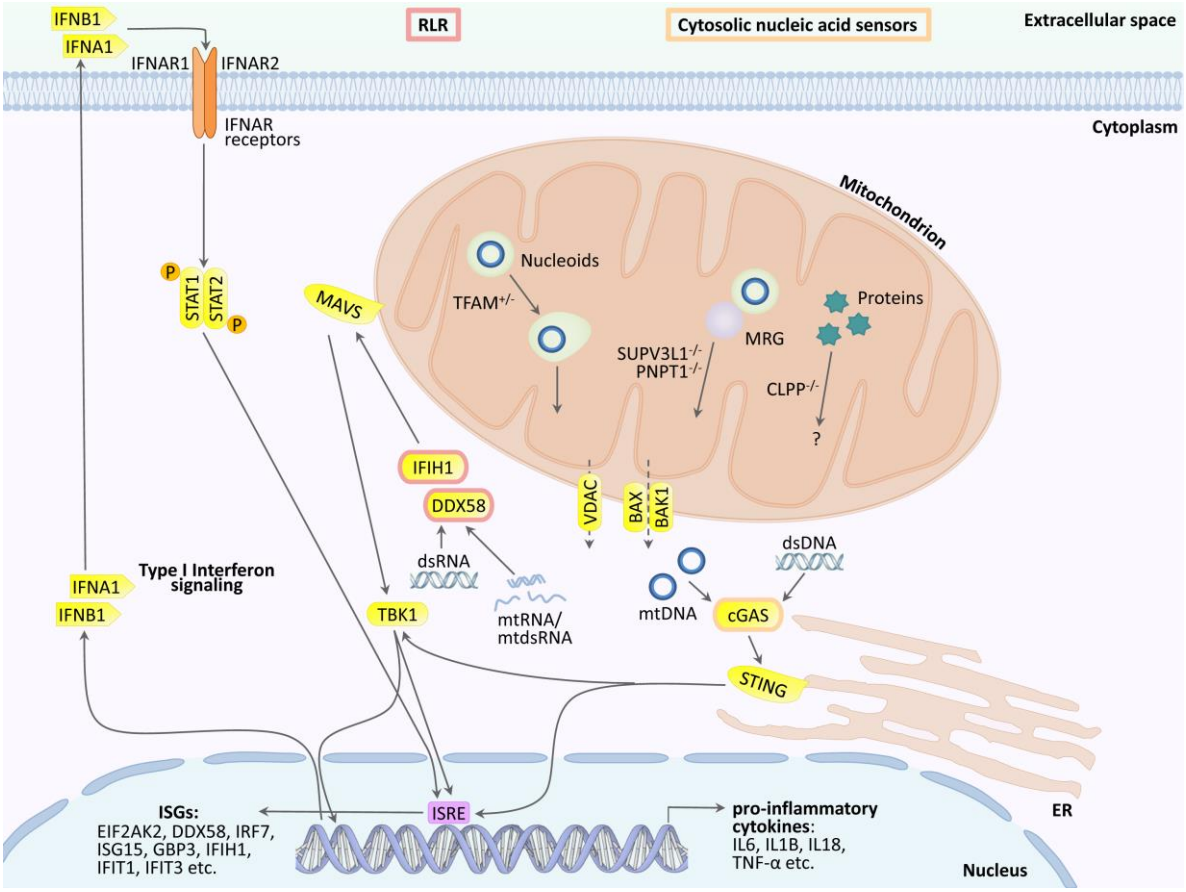

Figure 1. Innate immunity activation due to mutations in mitochondrial factors is mediated in the cytosol via the cGAS/STING pathway (when accumulated mtDNA is extruded to the cytosol) or the DDX58/IFIH1/MAVS sensors in the pattern recognition RLR pathway (when accumulated mitochondrial double-strand RNA is extruded). They stimulate the nuclear induction of interferon type I signaling. It is unclear if these established mechanisms also are prominent in ClpP-deficient cells, or additional pattern recognition receptors (TLR, NLR) and other cytosolic sensors play a relevant role. MRG = mitochondrial ribosomal granule; VDAC = PORIN; DDX58 = RIG-I; IFIH1 = MDA-5; STING = STING1, also known as TMEM173; ISRE = interferon-stimulated response element in the promoter of nuclear genes; other symbols are defined in the abbreviation list.

Particularly for TFAM mutations, the mechanism of innate immune activation has been elucidated in detail. Heterozygous TFAM deficiency results in abnormal packaging of mtDNA nucleoids and their extrusion into the cytosol, where TFAM-associated U-turn DNA will nucleate

 doi:10.20944/preprints202105.0021.v1

cGAS dimers and activate STING/TBK1 to induce type I interferon. Similarly, deficiencies of the mitochondrial RNA helicase SUPV3L1 or the mitochondrial polynucleotide phosphorylase PNPT1 lead to accumulation of double-stranded RNA that is released to the cytosol through the BAX/BAK1 and VDAC pores, then acting via DDX58/IFIH1/MAVS/TBK1 to upregulate interferon-stimulated gene expression (see schematic overview in **Figure 1**). These responses mediate resistance against microbial infections and enhance repair mechanisms that are also protective for the nuclear genome [18-24].

Not only does the rare Perrault syndrome show the combination of a primary mitochondrial dysfunction with subsequent sterile inflammation, but also the frequent neurodegenerative process in Parkinson's disease (PD) has this dual characteristic. Mutations in the PINK1 and PARKIN genes are responsible for juvenile-onset autosomal recessive PD variants of relatively mild progression [25]. Both factors are responsible for the autophagic degradation of damaged mitochondrial fragments [26]. Loss-of-function in this pathway leads not only to abnormal turnover of mitochondria, but also affects the cellular susceptibility to invasion by bacterial pathogens such as *Mycobacterium Tuberculosis* [27]. Mice with PINK1 or PARKIN mutations show consistent innate immune activation even in a special-pathogen-free environment or upon cell culture, and the depletion of the cytosolic immune coordinator STING can prevent the neurodegenerative process in such mice [28, 29].

An additional pathway how mitochondrial dysfunction can modulate innate immunity was recently demonstrated in fumarate hydratase deficient cells that exhibit excessively succinylated proteins in the mtDNA replication machinery, with progressive accumulation of mis-assembled nucleoids. Both fumarate and succinate are metabolites that are known to modulate the immune status of cells [30, 31].

It is also known that the metabolites ATP and cardiolipin, reactive oxygen species (ROS), N-formylated peptides, and enzymes such as Cytochrome C and Carbamoyl phosphate synthetase-1, upon their release from bacteria/mitochondria, may be sensed by eukaryotic hosts as damage-associated molecular patterns (DAMPs) and trigger the innate immune responses [32]. In addition, nuclear transcription factors are used to govern intra-mitochondrial processes, and sustained nuclear efforts to compensate mitochondrial anomalies may modulate also the expression of cytosolic factors and produce side-effects throughout the cell over time. As examples, transcriptional activity in mitochondria is controlled (i) via autofeedback from mitochondrial TFAM (UniProt database entry P40630-1) to a nuclear isoform of TFAM (Uniprot entry P40630-2) [33, 34], and via mitochondrial STAT1 that cross-talks with nuclear STAT1 [35]. It is well established that nuclear STAT1 has a massive impact on the innate immune response.

Our prior work has shown that the cGAS-STING pathway is primarily responsible for heightened activation of type I interferon production and downstream upregulation of interferon-stimulated genes in cells and tissues from ClpP-null mice [9]. However, it is possible that other alterations (i.e. accumulation of unfolded proteins in mitochondria with release of N-formyl peptides, a profoundly altered metabolite profile, and/or extruded mitochondrial RNA with hypomethylation, nucleotide chains in supercoil structure) could further enhance innate immune activation in ClpP-null mice. In view of clinical consequences like the resistance of ClpP-null mice against ulcerative dermatitis with lethal outcome [10], we tried to elucidate the molecular mechanisms how altered UPR^{mt} can activate innate immunity, examining some interplay of mitochondrial / nuclear protein isoforms as well as specifying the most affected DAMP-sensing pathways. Our data document strong accumulations for DNAJA3 (also known as TID1) and STAT1, intra-mitochondrially and extra-mitochondrially. These proteins are both known to modulate innate immunity, and were observed to interact physically [36, 37]. DNAJA3 was previously shown to be co-regulated with ClpP in the mitochondrial unfolded protein response pathway and might be a degradation substrate of ClpP or co-accumulate with such substrates in the mitochondrial matrix. It is possible that its impaired turnover would affect JAK-STAT signaling and modulate interferon signaling [22, 38]. In addition to the established inflammatory effects of mtDNA / mtdsRNA extrusion from mitochondria, this additional pathway might be ClpP-specific. The activation of innate immunity comprised a strong transcriptional induction of specific interferon-stimulated genes and cytosolic nucleic acid sensors

 doi:10.20944/preprints202105.0021.v1

(higher number of RNA sensors than of DNA sensors), as well as several pattern recognition receptor families (number of elevated factors in RLR > TLR >> NLR).

2. Materials and Methods

2.1 Mouse breeding

Homozygous *ClpP*$^{-/-}$ and wild-type (WT) mice were generated as littermate offspring from heterozygous breeders. They were genotyped at postnatal day 10 by ear-punches, and immediately after weaning pairs of mutants with age-/sex-matched WT controls were housed together, aged and dissected as reported before [10]. The mice used were kept under FELASA-certified conditions at the Central Animal Facility (ZFE) of the Goethe University Medical Faculty in Frankfurt. All animal experiments were carried out in accordance with the German Animal Welfare Act and with approval of the local animal authorities (Regierungspräsidium Darmstadt, FK/1073).

2.2 Mouse Embryonic Fibroblast Generation and Culture

Generation and culture of mouse embryonic fibroblasts (MEFs) were done as previously described [11]. Following intercrosses of *ClpP*$^{+/-}$ mice, WT and *ClpP*$^{-/-}$ MEFs were prepared from individual embryos at 14.5 days post-coitus. Cells were cultivated in Dulbecco's modified Eagle medium (DMEM) (Gibco, Thermo Fisher Scientific, Waltham, MA, USA) supplemented with 15% fetal bovine serum (FBS) (Gibco, Thermo Fisher Scientific) and 1% L-glutamine (Gibco, Thermo Fisher Scientific) at 37 °C and 5% CO_2 in a humidified incubator.

2.3 Mouse brain native gel electrophoresis and complexome profiling

Sample preparation [39] and high-resolution native electrophoresis (hrCNE) [40] of brain tissue were essentially done as described. Briefly: Brains were taken and further disrupted using a pre-cooled motor-driven glass/Teflon Potter-Elvehjem homogenizer at 2000 rpm and 40 strokes. Homogenates were centrifuged for 15 min at 600 g to remove nuclei, cell debris, and intact cells. Mitochondrial membranes were sedimented by centrifugation of the supernatant for 15 min at 22,000 g. Mitochondria-enriched membranes from 10 mg brain tissue were resuspended in 35 µl solubilization buffer (50 mM imidazole pH 7, 50 mM NaCl, 1 mM EDTA, 2 mM aminocaproic acid) and solubilized with 20 µl 20% digitonin (Serva, Heidelberg, Germany). Samples were supplemented with 5 µl 0.1% Ponceau S in 50% glycerol. Equal protein amounts of samples were loaded on top of a 3% to 18% acrylamide gradient gel (dimension 14x14 cm). After native electrophoresis in a cold chamber, native gels were fixed in 50% (v/v) methanol, 10% (v/v) acetic acid, 10 mM ammonium acetate for 30 min and stained with Coomassie (0.025% Serva Blue G, 10% (v/v) acetic acid) or blotted onto PVDF membranes and used for antibody decoration using an antibody against NDUFB8 and MitoProfile Total OXPHOS Rodent WB Antibody Cocktail (Mitosciences, Eugene, Oregon, USA). Coomassie-stained lanes were fractionated in 60 even pieces and digested with trypsin and subsequently analyzed by mass spectrometry. Experimental details and data were deposited to dataset identifier PRIDE: PXD025478.

2.4 Reverse Transcriptase Real-Time Quantitative PCR

As described in previous studies [10] and following manufacturers' instructions, total RNA isolation from MEFs and brain tissues was performed with TRI reagent (Sigma-Aldrich, St. Louis, MO, USA), and reverse transcription by SuperScript IV VILO Master Mix (Thermo Fisher Scientific). RT-qPCR was carried out with TaqMan® Gene Expression Assays (Thermo Fisher Scientific) in cDNA from 10 ng total RNA in 10 µl reactions with 2x Master Mix (Roche, Basel, Switzerland and Thermo Fisher Scientific) in a StepOnePlus Real-Time PCR System (Applied Biosystems, Thermo Fisher Scientific). The data was analyzed with the $2^{-\Delta\Delta CT}$ method [41]. To verify the null mutation in used tissue and MEF samples, RT-qPCR assays of *ClpP* normalized to *Tbp* were performed, in

 doi:10.20944/preprints202105.0021.v1

addition to the genotyping of each animal. The following TaqMan assays (Thermo Fisher Scientific) were employed to quantify the individual mRNA levels: *Aim2*- Mm01295719_m1, *ClpP*- Mm00489940_m1, *Ddx58*- Mm01216853_m1, *Dnaja3*- Mm00469723_m1, *Eif2ak2*- Mm01235643_m1, *Gbp3*- Mm00497606_m1, *Ifi204*- Mm00492602_m1, *Ifi205b (=Mnda)*- Mm04204353_mH, *Ifi35*- Mm00510329_m1, *Ifi44*- Mm00505670_m1, *Ifih1*- Mm00459183_m1, *Ifit1* (= *Isg56*)- Mm00515153_m1, *Ifit3*- Mm01704846_s1, *Ifna1*- Mm03030145_gH, *Ifnb1*- Mm00439552_s1, *Irf3*- Mm00516784_m1, *Mavs* (=*Ips-1*)- Mm00523170_m1, *Mb21d1 (=cGas)*- Mm01147496_m1, *Nfkb1*- Mm00476361_m1, *Nlrp3*- m00840904_m1, *Nlrx1*- Mm00617978_m1, *Oas1b*- Mm00449297_m1, *Oasl2*- Mm00496187_m1, *Rsad2*- Mm00491265_m1, *Stat1*- Mm00439531_m1, *Stat2*- Mm00490880_m1, *Supv3l1*- Mm00619586_m1, *Tbp*- Mm00446973_m1, *Tlr3*- Mm01207404_m1, *Tlr9*- Mm00446193_m1, *Tmem173*- Mm01158117_m1, *Trim25*- Mm01304226_m1, *Trim30a*- Mm00493346_m1, *Trim56*- Mm01207494_m1, *Tspan6*- Mm00451045_m1.

2.5 Quantitative Immunoblotting

Protein extraction and sample preparation from brain tissues and MEFs were carried out as described before [10, 42]. Samples of 20 µg of total protein were mixed with 2x loading buffer [250 mM Tris/HCl (pH 6.9), 20% glycerol, 4% SDS, 10% β-mercaptoethanol, 0.01% bromophenolblue, 5% MilliQ water], heated at 90 °C for 5 min and afterward separated in 8%, 10%, 12% or 15% tris-glycine polyacrylamide gels depending on the size of the investigated protein. Precision Plus Protein™ All Blue Standards (Bio-Rad, Hercules, CA, USA) was used as a size marker. Following the gel electrophoresis, protein transfer to nitrocellulose membranes (Bio-Rad) was done at 50 V over 90 min. The membranes were blocked in 5% BSA/TBS-T for 1 h at room temperature (RT) and incubated over night at 4 °C with primary antibodies against ClpP (1:1000, Proteintech, Rosemont, IL, USA, 15698-1-AP), DDX58 (1:1000, Cell Signaling, Danvers, MA, USA, #3743S), DNAJA3 (1:500, Cell Signaling, #4775), IFIT3 (1:800/1:1000, Proteintech, 15201-1-AP), IκBα (1:1000, Cell Signaling, #4814), IKKα (1:500, Cell Signaling, #11930), IKKβ (1:1000, Cell Signaling, #8943), IRF3 (1:1000, Cell Signaling, #4302), IRF7 (1:1000, Abcam, Cambridge, UK, ab109255), ISG15 (1:1000, Invitrogen, PA5-17461), NFκB P65 (1:1000, Cell Signaling, #8242), Phospho-IKKα/β (1:800, Cell Signaling, #2697), Phospho-IκBα (1:1000, Cell Signaling, #2859), STAT1 (1:1000, Cell Signaling, #9172), SUPV3L1 (1:800/1:1000, MyBioSource, San Diego, CA, USA, MBS9130033), TLR9 (1:800, Novus B, Centennial, CO, USA, NBP2-24729), TRIM25 (1:1000, Abcam, ab167154). As secondary antibodies, fluorescence-labeled anti-rabbit or anti-mouse antibodies (1:15,000, Thermo Fisher Scientific, Invitrogen) were used. The fluorescence was detected by using the Li-Cor Odyssey Classic Instrument and was densitometrically analyzed with Image Studio Lite Version 5.2 (Li-Cor Biosciences). Bands were normalized against β-ACTIN (= ACTB) (1:10,000, Sigma-Aldrich, A5441). For fractionation experiments GAPDH (1:10,000, Sigma-Adrich, Taufkirchen, Germany, #CB1001), LAMIN A/C (1:1000, Abcam, #AB169532) or PORIN-1 (1:500, Cell Signaling, #4866) were used as loading controls.

2.6 Subcellular fractionation

Fractionation into nuclear, mitochondrial, and cytosolic fractions was done as follows: 4x10^6 MEF cells were collected with trypsin, centrifuged at 800 g for 3 min, washed with PBS, the centrifugation step was repeated, and the pellet was resuspended in 300 µl cytosol extract buffer (CEB). The suspension was shaken 5 min head-to-head at RT and centrifuged at 800 g for 3 min. The supernatant was stored as cytosolic fraction. The remaining pellet was washed once with CEB, centrifuged at 800 g for 3 min and then resuspended in 300 µl mitochondrial lysis buffer (MLB), shaken 10 min head-to-heat at RT and centrifuged at 800 g for 3 min. The supernatant was stored as mitochondrial fraction. The remaining pellet was washed once with MLB, centrifuged at 800 g for 3 min and then resuspended in 300 µl RIPA buffer. The suspension was sonicated, 10 min shaken head-to-head at RT and centrifuged at 800 g for 3 min. The supernatant was stored as nuclear fraction. Experiments were repeated with 3 WT and 3 *ClpP*$^{-/-}$ lines. Buffers were composed as follows:

CEB: (250 mM Sucrose, 70 mM KCl, 137 mM NaCl, 4.3 mM Na2HPO4, 1.4 mM KH2PO4, with freshly added 100 µM PMSF, 10 µg/ml leupeptin, 2 µg/ml aprotinin, 200 µg/ml digitonin)

MLB: (50 mM TRIS/HCl pH 7.4, 150 mM NaCl, 2 mM EDTA, 2 mM EGTA, 0.2% Triton X100, 0.3% NP40, with freshly added 100 µM PMSF, 10 µg/ml leupeptin, 2 µg/ml aprotinin)

RIPA buffer: [50 M TRIS/HCl pH 8.0, 150 mM NaCl, 0.1% SDS, 1% triton, 0.5% sodium deoxycholate, 2 mM EDTA, protease inhibitor cocktail (Sigma Aldrich, St. Louis, Missouri, USA)]. All chemicals were purchased from Merck (Darmstadt, Germany) unless mentioned otherwise.

2.7 Statistical Evaluation

Statistical analysis of quantitative immunoblot and RT-qPCR results were conducted by using GraphPad Prism (Version 8.4.2, GraphPad, San Diego, CA, USA) with unpaired Student's t-tests. Results including standard error of the mean (SEM) and p values (p= probability) were visualized in bar graphs, with the following significances illustrated by asterisks or symbols: * (or #/§) $p < 0.05$; ** (or ##/§§) $p < 0.01$; *** (or ###/§§§) $p < 0.001$; **** (or ####/§§§§) $p < 0.0001$; not significant (ns) $p > 0.05$; tendency (T) $0.05 < p < 0.1$.

2.8 Visualization

Graphs were generated by using GraphPad Prism (Version 8.4.2).

3. Results

3.1. Protein mass spectrometry analysis of mitochondrial matrix unfolded protein response factors by complexomics reveals prominent assembly anomalies for DNAJA3 in ClpP$^{-/-}$ mouse brain.

To understand the cumulative effects of chronic ClpP deficiency on the UPR^{mt} pathway in brain tissue with its postmitotic neurons during the aging process, dissected brains from 12-month-old *ClpP*$^{-/-}$ and sex-matched littermate control mice were homogenized and centrifuged to obtain mitochondria-enriched membranes. High-resolution native electrophoresis was used to resolve protein complex assemblies, and then their components were identified and quantified by mass spectrometry (**Figure 2**). A selective analysis of UPR^{mt} factors demonstrated the absence of ClpP (monomer with size 29 kDa), as well as pronounced accumulations for the disaggregase ClpX (69 kDa), and the Hsp90-homologous molecular chaperone TRAP1 (size 80 kDa). Interestingly, accumulation with additional disperse migration at abnormally high molecular weights was evident for the Hsp70-homologous chaperone HSPA9 (Mortalin, 73 kDa), its GrpE-homologous co-chaperone GRPEL1 (24 kDa), and even more so for its DnaJ-homologous co-chaperone DNAJA3 (52 kDa for large isoform precursor, 49 kDa for small isoform precursors). DnaJ was originally identified in *E. coli* bacteria as a factor required for the replication of bacterial and viral DNA [43]. Given that DNAJA3 is known as protein interactor of STAT1 and as modulator of inflammatory responses also via NFκB [22, 36, 37, 44-47], we tested if STAT1 dysregulation also occurred in ClpP deficient tissue. Given that brain anomalies might be caused by the innate immune system or the adaptive immune system, we decided to perform further studies in primary fibroblast cultures taken at early embryonic age from *ClpP*$^{-/-}$ mice and their sex-matched littermate controls, comparing these results with data from brain samples at two ages.

Preprints (www.preprints.org) | NOT PEER-REVIEWED | Posted: 4 May 2021 doi:10.20944/preprints202105.0021.v1

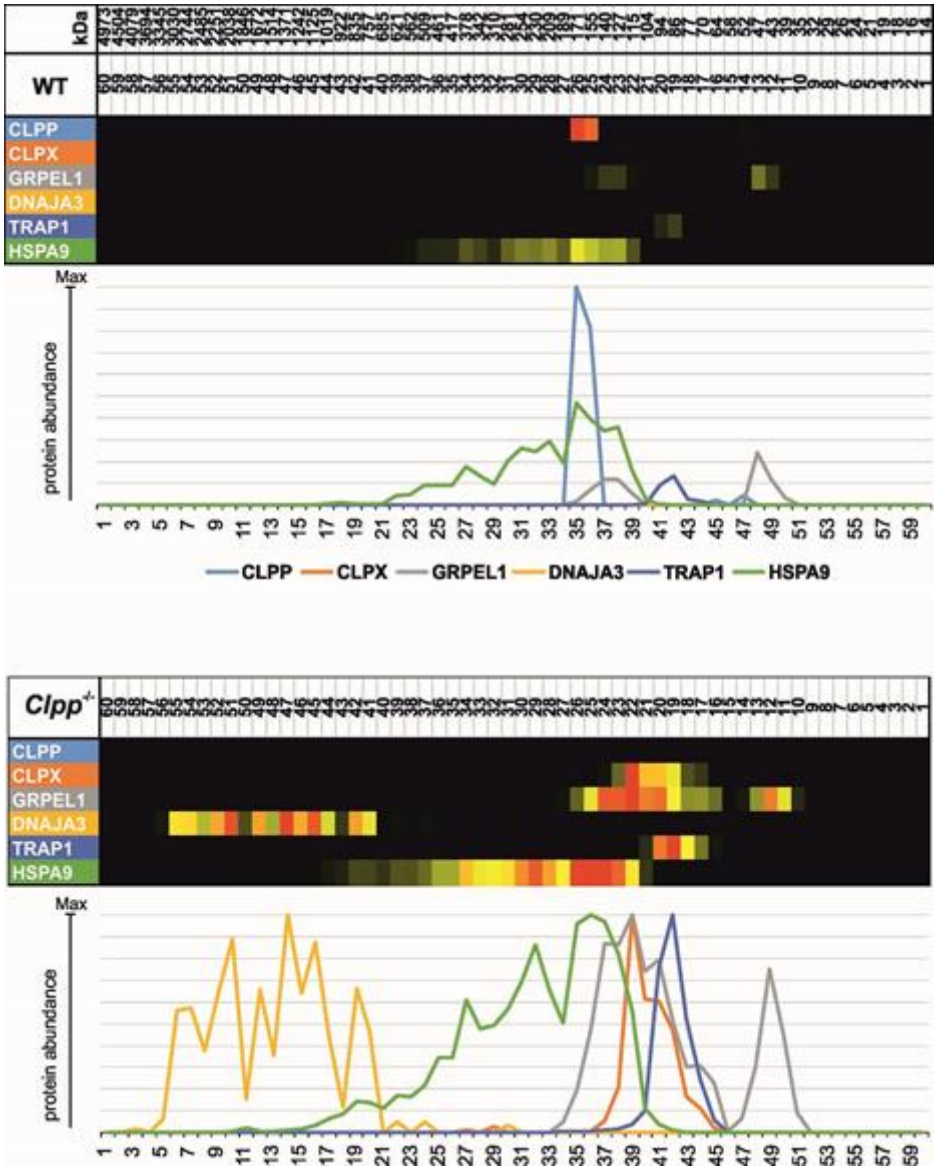

Figure 2. Complexome profile of mitochondrial matrix chaperones in ClpP$^{-/-}$ brain. Digitonin-solubilized mitochondrial complexes were separated by high resolution clear native electrophoresis (hrCNE) into 60 fractions and identified/quantified by mass spectrometry. Protein complexes in Coomassie-stained gels were further processed to present abundance profiles as heatmap (with red > yellow color representing highest abundance) and 2D plot (with each protein represented by differently colored line as coded in gel picture above). The absence of ClpP is clearly detected, and triggers not only marked accumulation of several downstream factors in the UPR^{mt} pathway, but also abnormal migration at unexpected high molecular sizes, particularly for the strongly accumulated co-chaperone DNAJA3.

3.2. *Verification of ClpP$^{-/-}$ in MEFs, with analysis of mitochondrial DNA and RNA associated factors*

First, the genetic *ClpP*-ablation was verified at mRNA and protein level by using immunoblots (**Figure 3A**) and RT-qPCRs (**Figure 3B**). Its deficiency was documented in MEFs and the brain samples used.

With quantitative immunoblots, a strong accumulation was again found for DNAJA3 (**Figure 3C**). This observation was not explained by transcriptional induction (**Figure 3D**), so it might simply represent a marker of protein complex assembly problems that result in slowed turnover and degradation of DNAJA3 targets.

 doi:10.20944/preprints202105.0021.v1

Our previous work has demonstrated ClpP-null cells to display mitochondrial nucleoid assembly problems and extrude mtDNA into the cytosol [9]. In view of the parallel disturbance of mitoribosome assembly via dysregulation of the RNA chaperone ERAL1 in ClpP-null cells [8], it is conceivable that mtRNA gets also extruded into the cytosol. Although mtDNA was shown to be the main trigger of innate immunity activation in ClpP-cells, given that cGAS and STING deficiency reduced the induction of interferon-stimulated genes almost to WT levels [9], it is possible that other mtDAMPs could participate in the elevated innate immune responses of ClpP-null cells. The RNA helicase SUPV3L1, a protein component of the mitochondrial degradosome that was implicated in the mitochondrial release of mtdsRNA [24], showed a significant reduction of protein abundance (**Figure 3E**) in MEFs, while its transcripts were not reduced. Selectively in brain tissue of 11-19 month old mice the *Supv3l1* mRNA levels were significantly diminished (**Figure 3**F). It is difficult to know if these slight deficits are meaningful, but clearly, a strong induction of this helicase in response to mtdsRNA pathology was not detected.

Preprints (www.preprints.org) | NOT PEER-REVIEWED | Posted: 4 May 2021 doi:10.20944/preprints202105.0021.v1

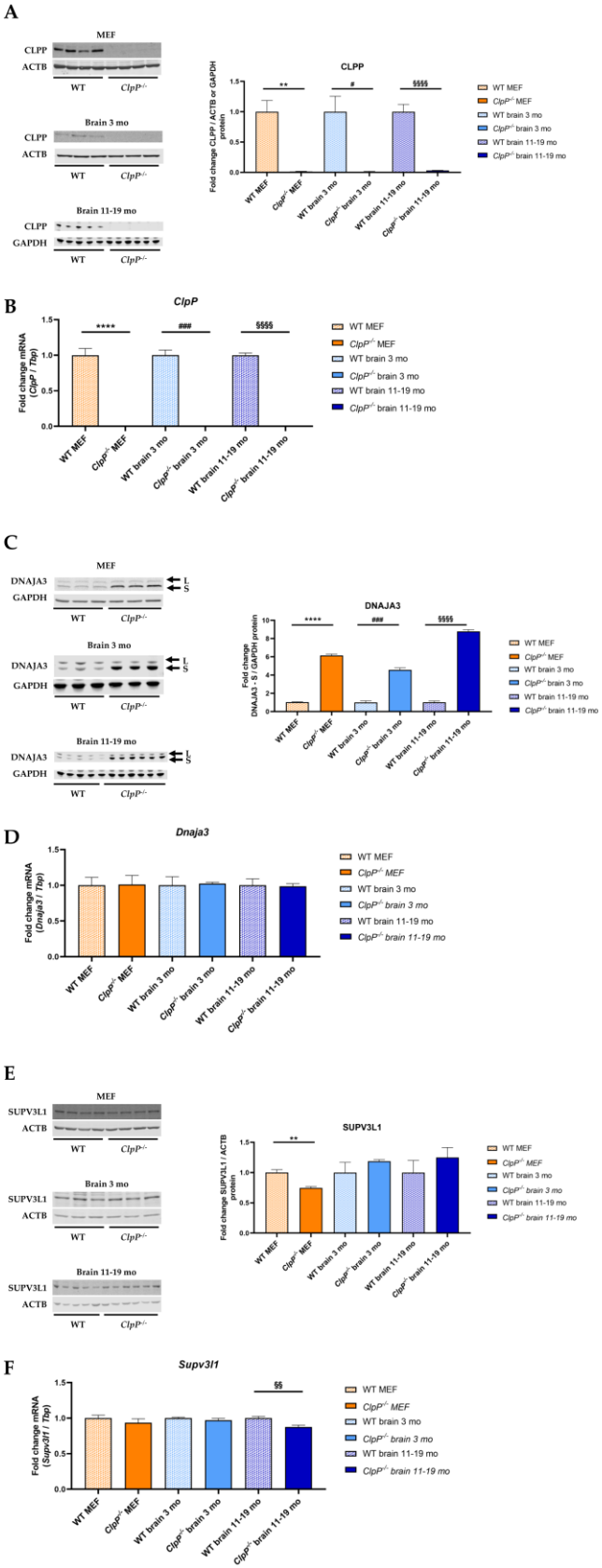

Figure 3. Verification of *ClpP*$^{-/-}$ genotype via **(A)** quantitative immunoblots and **(B)** RT-qPCRs in MEF and brain tissue of 3 and 11-19 month-old mice. Analysis of **(C)** DNAJA3 protein and **(D)** mRNA levels, as well as **(E)** SUPV3L1 protein and **(F)** mRNA levels, both in MEF and brain tissue of 3 and

Preprints (www.preprints.org) | NOT PEER-REVIEWED | Posted: 4 May 2021 doi:10.20944/preprints202105.0021.v1

11-19 month-old mice. Immunoblots were normalized to ACTB or GAPDH, RT-qPCRs to *Tbp* levels. Data are presented as mean ± SEM. WTs are shown as checked, ClpP-/- as plain colored bar graphs. Significances are illustrated by symbols: ** or §§ $p < 0.01$; ### $p < 0.001$; **** or §§§§ $p < 0.0001$; not significant (ns) $p > 0.05$. Asterisks portray significant differences between WT and ClpP$^{-/-}$ MEF, hashtags show significant effects in 3-month-old brain tissue between WT and *ClpP*$^{-/-}$ mice, and section signs visualize significant differences in brain tissue from 11-19 month-old mice, between WT and *ClpP*$^{-/-}$ genotype. WT MEF: n= 4-5; *ClpP*$^{-/-}$ MEF: n= 3-5; WT brain 3 months: n= 3; *ClpP*$^{-/-}$ brain 3 months: n= 3; WT brain 11-19 months: n= 5; *ClpP*$^{-/-}$ brain 11-19 months: n= 6.

3.3. Cell fractionation demonstrates ClpP-deficiency to increase cytosolic STAT1 and nuclear DNAJA3

To elucidate how ClpP deficiency and UPR^{mt} pathology signal retrogradely to dysregulate factors with nuclear function such as the transcription factor STAT1, already at embryonal stage in fibroblasts, the fractionation of different subcellular compartments by sequential protein extraction with appropriate detergents was done. Enrichment of the mitochondrial fraction was assessed by PORIN as component of the main outer mitochondrial membrane multimeric pore, the cytosolic fraction was assessed by GAPDH as glycolytic enzyme, and the nuclear fraction by LAMIN A/C as component of the matrix on the inner surface of the nuclear envelope. Immunoblot detection with DNAJA3 antibodies showed an accumulation for the mitochondrially imported and cleaved small isoform not only in the *ClpP*$^{-/-}$ mitochondrial fraction, but also in the *ClpP*$^{-/-}$ nuclear fraction a band of very similar size was accumulated (**Figure 4A**). Accumulation of the DNAJA3 small isoform in the *ClpP*$^{-/-}$ mitochondrial fraction was also observed on membranes where more protein was loaded per lane, in a comparison to cytosolic fraction (**Figure 4B**), but DNAJA3 was below the detection threshold in the cytoplasm. In contrast, STAT1 immunoproduct of the predicted size accumulated in *ClpP*$^{-/-}$ mitochondrial fraction and in *ClpP*$^{-/-}$ cytosolic fraction (**Figure 4B**), but STAT1 was below the detection threshold in the nuclear fraction, possibly due to insufficient solubilization from DNA complexes (**Figure 4A**). It is known that ClpP-null cells have elevated levels of mis-assembled mtDNA [9, 10], so it seems appropriate to observe responses of a mammalian homolog of DnaJ chaperones which are known to control bacterial and viral DNA replication [43, 48], and of STAT1 that represses mitochondrially encoded transcripts [35]. Importantly, these responses involve not only intra-mitochondrial DNAJA3 and STAT1 but extend to extra-mitochondrial compartments.

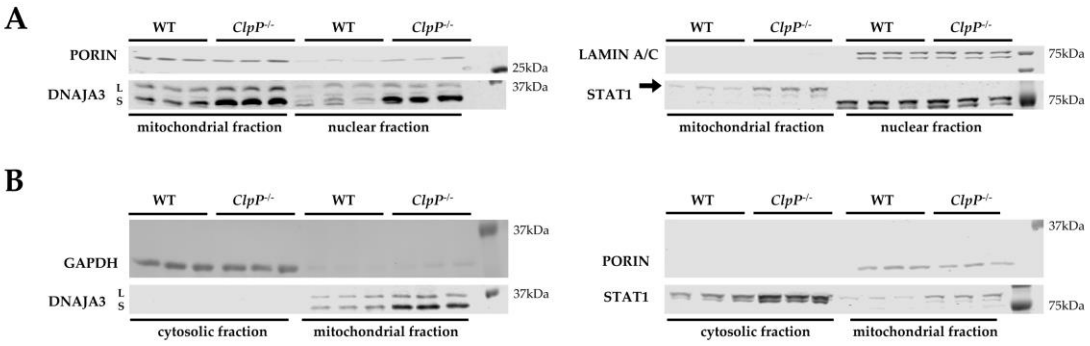

Figure 4. Cell fractionation in MEFs, comparing mitochondrial with nuclear (A) and cytosolic (B) compartments. Immunoblotting was used to control the purity of the fractionation with the mitochondrial marker PORIN, the nuclear marker LAMIN A/C, and the cytosolic marker GAPDH, comparing littermate WT and *ClpP*$^{-/-}$ cells of matched sex. The detection of DNAJA3 revealed ClpP deficiency to cause accumulation of DNAJA3 short isoform (S) in mitochondria and nucleus, while STAT1 (87 kDa) accumulation occurred in mitochondria and cytosol.

 doi:10.20944/preprints202105.0021.v1

3.4. Transcriptional analysis of induced ISGs, PRRs and associated factors

In view of published global transcriptome evidence of increased antiviral defenses in ClpP-null mice, we wanted to further characterize the signaling pathways involved [9-11]. Therefore, mRNA expression levels of relevant transcription factors, interferon-stimulated genes, cytosolic DAMP sensors, and pattern recognition receptors (PRRs) with associated factors were surveyed by RT-qPCR (**Figure 5**).

Several investigated inflammatory transcription factors and interferon-stimulated genes (*Stat1*, *Stat2*, *Ifi35*, *Ifi44*, *Gbp3*) showed significantly increased mRNA levels (**Figure 5A**). A very strong induction was detected especially for *Ifi44*, with effect sizes of 7.257-fold in the brain of 11-19 month-old ClpP-null mice and 11.11-fold in MEFs. The PRRs lead to an induction of interferon-stimulated genes (ISGs), via type-I interferons (IFN-I) and other pathways. Some of the ISGs are the PPRs themselves, which may lead to an effect of self-induction. Other ISGs also exert anti-pathogenic functions in the context of the innate immune system. The main IFN-I transcripts, *Ifna1* and *Ifnb1*, showed only partially significant inductions (Error! Reference source not found.**A**). While both were significantly upregulated in MEFs, only *Ifnb1* was induced in the 11-19 month-old ClpP-null mice brain tissue samples.

Prominent significant upregulations were also found for a number of cytosolic nucleic acid sensors (*Ifit1*, *Ifit3*, *Oas1b*, *Ifi204*, *Mnda*, with lesser induction for *Eif2ak2=Pkr* and for *Aim2=Pyhin4*) (**Figure 5B,C**), and the retinoic acid inducible gene like receptors (RLRs) (*Ddx58=Rig-I*, *Ifih1*) with their associated factors (*Oasl2*, *Trim25*) (**Figure 5D**). No significant transcriptional changes were apparent in the cGAS-STING signaling pathway, with STING mRNA here referred to as *Tmem173*, consistent with previous observations that the regulation of this pathway occurs via dimerization and phosphorylation (**Figure 5C**). Nonetheless, *Trim56* mRNA levels showed a 1.473-fold induction in 11-19 month-old ClpP-null mice. TRIM56 protein can induce cGAS and therefore the downstream signaling pathway [49]. Although a 2.261-fold induction of *Ddx58* and a 2.016-fold induction of *Ifih1* were detected in the brain tissue of 11-19 month-old *ClpP*$^{-/-}$ mice (**Figure 5D**), the downstream mitochondrial adapter *Mavs* was not significantly altered in expression. Interestingly, toll-like receptors (TLRs) showed fewer transcriptional inductions (**Figure 5E**), and nuclear oligomerization-domain like receptors (NLRs) almost none (**Figure 5F**). In young brains, only *Trim30a* levels were significantly increased (**Figure 5E**). In contrast to that, the interferons *Ifna1* and *Ifnb1*, as well as *Nfkb1* and *Irf3* did not show transcriptional activation (**Suppl. Figure S1A-C**).

Preprints (www.preprints.org) | NOT PEER-REVIEWED | Posted: 4 May 2021 doi:10.20944/preprints202105.0021.v1

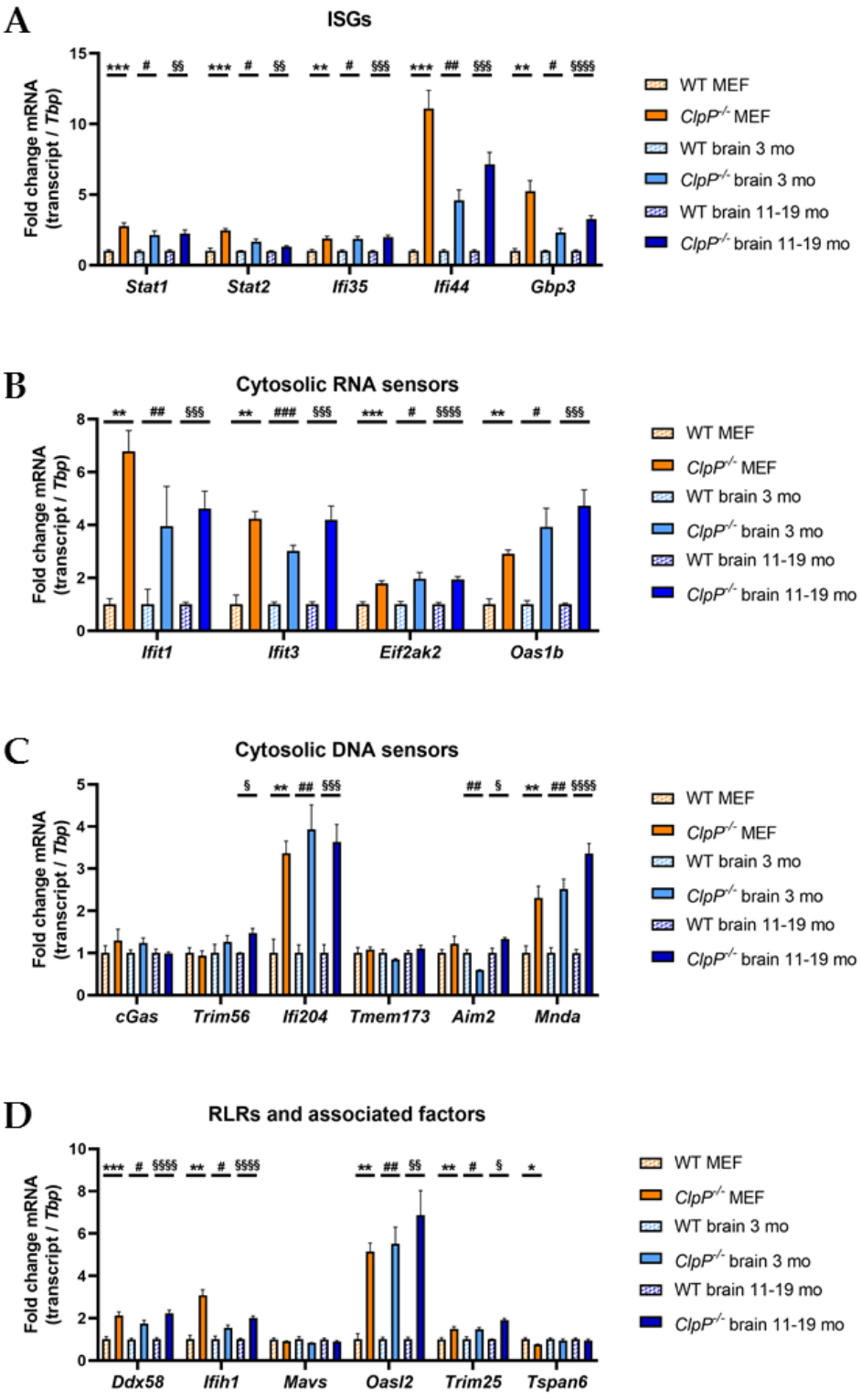

Preprints (www.preprints.org) | NOT PEER-REVIEWED | Posted: 4 May 2021 doi:10.20944/preprints202105.0021.v1

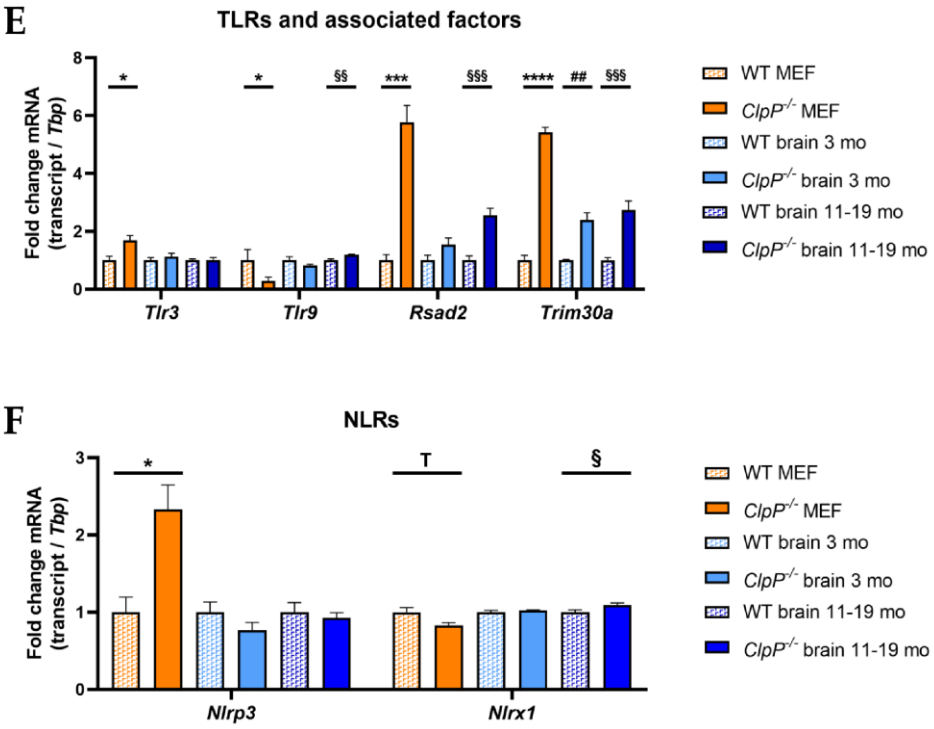

Figure 5. Analysis of mRNA expression by RT-qPCR in MEFs and brain tissue of 3 and 11-19 month-old mice, focusing on **(A)** induced interferon-stimulated genes, **(B)** cytosolic RNA sensors, **(C)** cytosolic DNA sensors, **(D)** RLRs with associated factors, **(E)** TLRs with associated factors, and **(F)** NLRs. RT-qPCRs were normalized to *Tbp* levels. Data are presented as mean ± SEM. WTs are shown as checked, *ClpP*$^{-/-}$ as plain colored bar graphs. Statistical tendencies and significances are illustrated by symbols: * or #/§ $p < 0.05$; ** or ##/§§ $p < 0.01$; *** or ###/§§§ $p < 0.001$; **** or §§§§ $p < 0.0001$; not significant (ns) $p > 0.05$; tendency (T) $0.05 < p < 0.1$. Asterisks portray significant differences between WT and *ClpP*$^{-/-}$ MEF, hashtags illustrate significant effects in brain tissue between 3-month-old WT and *ClpP*$^{-/-}$ mice, and section signs visualize significant differences in brain of 11-19 month-old WT versus *ClpP*$^{-/-}$ mice. WT MEF: n= 3-9; *ClpP*$^{-/-}$ MEF: n= 3-8; WT brain 3 months: n= 3; *ClpP*$^{-/-}$ brain 3 months: n= 3; WT brain 11-19 months: n= 5; *ClpP*$^{-/-}$ brain 11-19 months: n= 5-6.

3.5 Quantitative Immunoblots of induced transcription factors, ISGs, nucleic acid sensors and PRRs

To validate the significant and strong transcript dysregulation at the protein level, quantitative immunoblots were employed whenever sufficiently specific and sensitive antibodies were available commercially. The significantly elevated abundances of STAT1, IFIT3, DDX58, TRIM25, and ISG15 in ClpP-null MEFs confirmed the activation of the innate immune defenses from embryonal stage, independent from the adaptive immune system (**Figure 6**). The significantly elevated abundances of STAT1, DDX58 and ISG15 in the brains of 3-month-old ClpP-null mice demonstrated this neuroinflammation to precede neural phenotypes, given that Perrault syndrome features such as hearing loss, ataxia and white matter degeneration in mice do not appear before ages around 12 months [10]. The even stronger increases of STAT1, IFIT3, and DDX58 abundance in brain of 11-19 month-old ClpP-null mice indicate that their levels correlate with the progression of sterile neuroinflammation. Other factors in the innate immune sensing pathways, such as the interferons IRF3 and IRF7, several NFκB-associated factors and TLR9 did not exhibit elevated abundance (**Suppl. Figure S1C-E**).

Preprints (www.preprints.org) | NOT PEER-REVIEWED | Posted: 4 May 2021 doi:10.20944/preprints202105.0021.v1

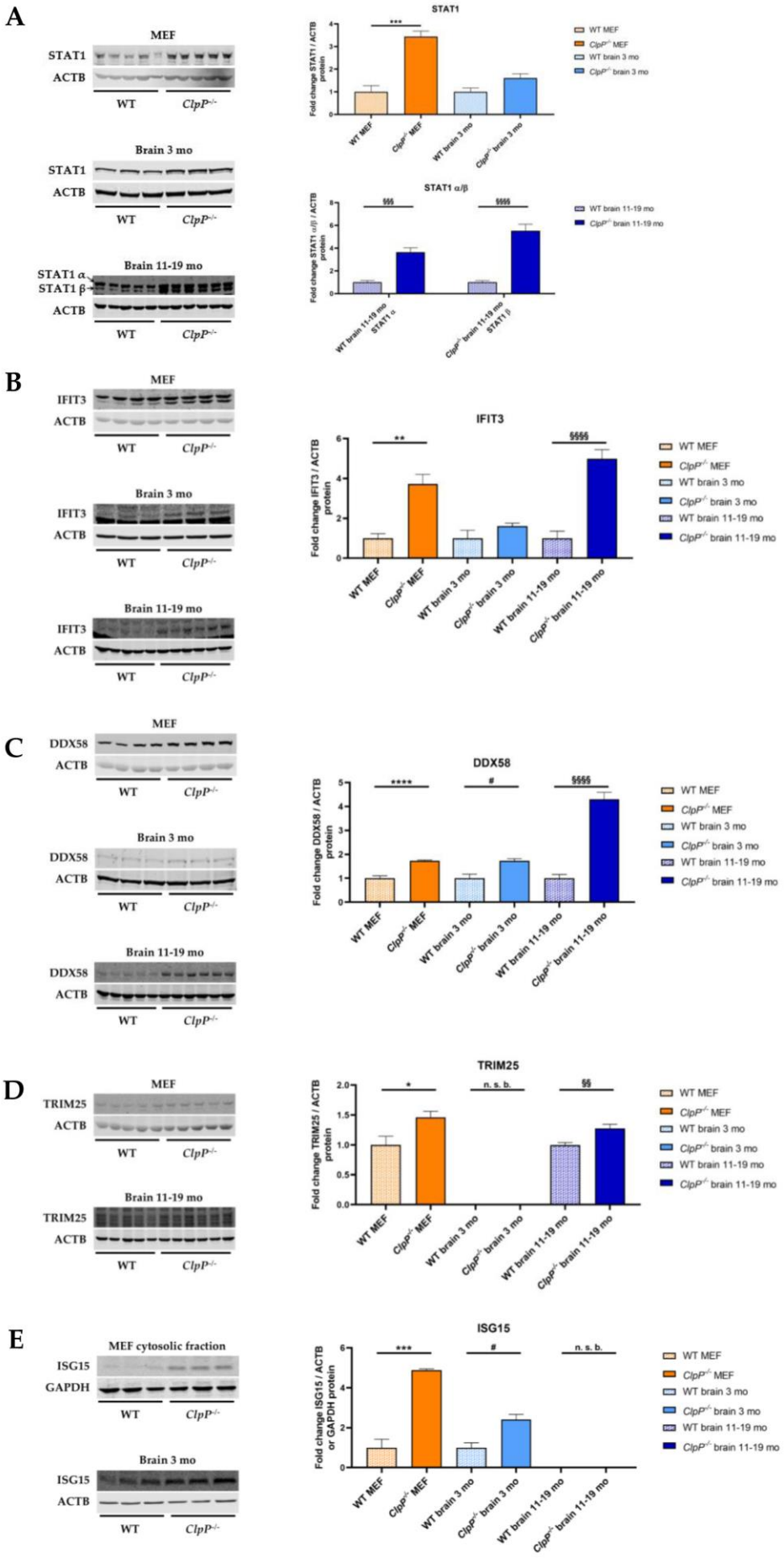

 doi:10.20944/preprints202105.0021.v1

Figure 6. Analysis of protein expression by quantitative immunoblots for **(A)** the transcriptional immune modulator STAT1, **(B)** the cytosolic RNA sensor IFIT3, as well as the RLR pathway components **(C)** DDX58, **(D)** TRIM25 and **(E)** ISG15, in MEFs and brain from 3 versus 11-19 month-old mice. Immunoblots were normalized to ACTB or GAPDH. Data are presented as mean ± SEM. In bar graphs, WT is shown as checked, while *ClpP*$^{-/-}$ as plain colored. Statistical significances are illustrated by symbols: * or # $p < 0.05$; ** or §§ $p < 0.01$; *** or §§§ $p < 0.001$; **** or §§§§ $p < 0.0001$; not significant (ns) $p > 0.05$. Asterisks portray significant differences between WT and *ClpP*$^{-/-}$ MEFs, hashtags show significant effects in brain between 3-month-old WT and *ClpP*$^{-/-}$ mice, and the section sign visualizes significant differences in brain from 11-19 month-old WT versus *ClpP*$^{-/-}$ mice. n. s. b.= no specific bands. WT MEF: n= 3-5; *ClpP*$^{-/-}$ MEF: n= 3-5; WT brain 3 months: n= 3; *ClpP*$^{-/-}$ brain 3 months: n= 3; WT brain 11-19 months: n= 5; *ClpP*$^{-/-}$ brain 11-19 months: n= 6.

4. Discussion

Attempting to elucidate the molecular pathways how the deficiency of ClpP as a key molecule in the UPR^{mt} triggers innate immune activation, the data obtained reflect a quite specific profile rather than a generic induction of interferon-stimulated genes, as is readily apparent by the comparison of the 2-fold induction of *Ifi35* mRNA versus the >10-fold induction of *Ifi44* mRNA (**Figure 5A**), or the comparison of the strong induction of many RLR factors with up to 7-fold effect size (**Figure 5D**) versus the singular induction of a NLR factor in MEFs (**Figure 5F**). This profile seems tuned to optimally detect immune-stimulatory dsDNA and dsRNA, by transcriptional activation of cytosolic DNA and RNA sensors, RLR pathway components, and ISGs. A detectable sensitization is also apparent towards ssRNA, while the sensing factors for muramyl dipeptides from Gram-negative bacteria appeared unchanged (**Figure 7**). We have previously shown by cGAS- and STING- depletion that the ISG induction depends mostly on the mtDNA [9], so the mtRNA extrusion to the cytosol would make only a minor contribution. The observation that many RNA sensors are activated may simply reflect a general antiviral program in view of the large number of very diverse RNA viruses. This scenario is known from TFAM heterozygous knockout cells, appears similarly strong in ClpP homozygous knockout cells, while it appears considerably weaker in PINK1/PARKIN mutants, when the expression upregulation levels and the delay in pathology onset are compared.

Preprints (www.preprints.org) | NOT PEER-REVIEWED | Posted: 4 May 2021 doi:10.20944/preprints202105.0021.v1

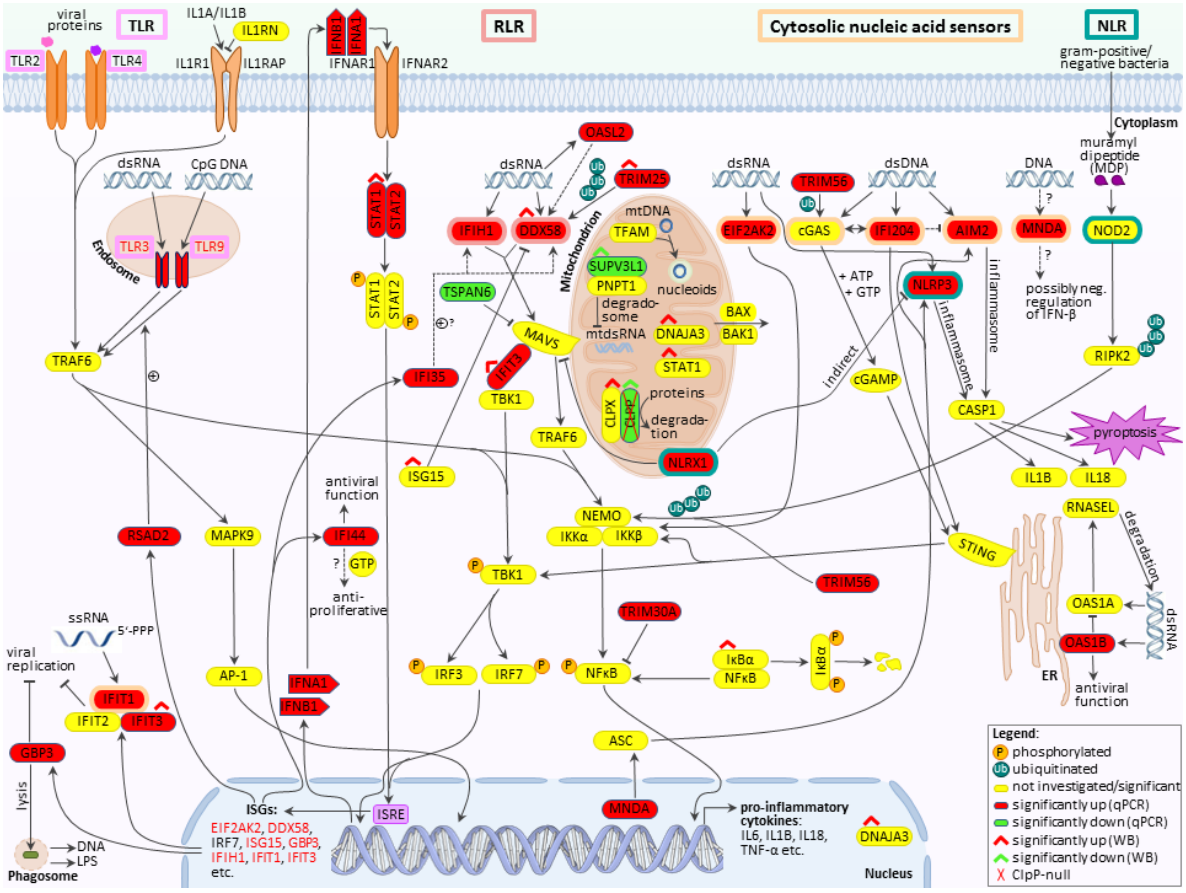

Figure 7. Schematic overview of innate immunity signaling, with illustration of the results from this study. TLRs= outlined in pink; RLRs= outlined in red; cytosolic nucleic acid sensors= outlined in orange; NLRs= outlined in green. Significant RT-qPCR results are represented by highlighting the factors in red, green or yellow (red= induced; green= reduced; yellow= not significant/investigated). Significantly altered protein expressions were marked with red or green roofs (red= increased; green= reduced). Dashed lines indicate discussed functions of corresponding factors. += induction; P= phosphorylated; Ub= ubiquitinated; other symbols are defined in the abbreviation list.

Thus, the molecular mechanisms involved in this innate immune activation by endogenous, immunostimulatory nucleic acids from mitochondria are not only relevant in the rare ClpP mutants. So far, the concept prevailed that the Perrault syndrome late manifestations of neurodegeneration and deafness are explained by the impaired translation fidelity in mitochondria, which leads to bioenergetics deficits [8, 50]. If mitochondrial mishandling of nucleic acid / protein complexes triggers innate immune activation and if the neuroinflammatory process is responsible for deafness, ataxia, and leukodystrophy in the later course of Perrault syndrome, then the therapeutic injection of antisense oligonucleotides to deplete STING as integrator of inflammatory signaling might have neuroprotective value. Preventive benefits of STING depletion have already been demonstrated in PINK1 and PARKIN mutants where the neurodegenerative process could be mitigated [29]. The therapeutic efficacy of antisense oligonucleotide (ASO) injections is impressive in patients and animal models with motor neuron degeneration [51, 52]. Our data permit the identification of additional therapeutic targets in these inflammatory signaling pathways. The relevance of neuroinflammation due to nucleic acid toxicity might also hold true for related disorders, where neurodegeneration is triggered by mutations in mitochondrial factors such as TWNK, POLG, TFB1M, MTRNR1, TRMU and GTPBP3, or in components of the mitochondrial and nuclear DNA repair pathway such as RRM2B, or in the cytosolic ribosomal translation machinery amino acid tRNA synthetases. This notion is consistent with the existence of autoimmune disorders where the tRNA synthetases are targeted specifically by autoantibodies, resulting in early-onset myopathy, interstitial lung

inflammation, skin rash, arthropathy and vasculitis [53-57]. Certainly in the autoimmune vasculitis variants known as Aicardi-Goutières syndrome, where altered degradation of cytosolic DNA or RNA is caused by mutations in TREX1 / SAMHD1 / RNASEH2A/B/C / ADAR / IFIH1 / PNPT1, the progressive immune activation leads to phenotypes of neuro-inflammation/-degeneration [58, 59]. Therefore, the late-onset progressive neuropathy, ataxia, and leukodystrophy in patients with ClpP mutations might be mediated by the innate immune activation. In contrast, the early-onset infertility could be due to meiosis defects, where the handling of nuclear DNA is impaired in similar ways as the handling of mitochondrial nucleoids in ClpP cells.

Not only the severity of inflammatory tissue destruction distinguishes the mutants in TFAM / ClpP / PINK1 / PARKIN, but also the selective massive affection of female and male meiosis upon ClpP loss-of-function, resulting in a complete infertility with azoospermia that is much more severe than the sperm motility impairment usually associated with bioenergetic respiratory or glycolysis failure. [55] Thus, there must be ClpP-specific effects extra-mitochondrially. One candidate seems to be the co-chaperone DNAJA3 that is mostly localized to the mitochondrial matrix, and particularly the short isoform normally has minimal cytosolic retention time, so physiologically only its long isoform would interact with the JAK-STAT pathway [37]. The findings above seem paradoxical, since DNAJA3 abundance increases in the nucleus, while STAT1 abundance is further enhanced in the cytosol. However, a scenario is conceivable where excessive amounts of DNAJA3 interfere with the correct disassembly of nuclear transcription factor complexes, thus overactivating *Stat1* gene transcription, while leading to compensatory efforts to retain STAT1 protein in the cytosol and minimize its unwanted overexpression. It is interesting to note a very recent report that the dysfunction of another mitochondrial DnaJ homolog known as DNAJC30, which appears to have a crucial role for the assembly/disassembly and turnover of the respiratory complex N-module, results in a neurodegenerative process that selectively affects the optical nerve [60]. It has previously never been understood how different gene mutations that result in impairment of mitochondrial function would have vastly different tissue-specific consequences, if bioenergetics deficits are the underlying problem. If differently tuned inflammatory consequences of each gene mutation are responsible for the long-term clinical consequences, then the tissue-specificity variance of mitochondrial pathology may be much easier to understand.

5. Conclusions

Overall, our investigation of ClpP-null brains and MEFs detected UPR^{mt} anomalies prominently for DNAJA3. Enhanced levels and redistribution were also observed for its interaction partner STAT1. Both were altered in the intra-mitochondrial and extra-mitochondrial compartments. These anomalies may be ClpP-specific, but perhaps they might also be found in other variants of Perrault syndrome. These DNAJA3 anomalies are followed by early-onset deafness in ClpP-mutant patients, while a recent report showed anomalies of the mitochondrial matrix chaperone DNAJC30 to occur in hereditary optic nerve atrophy, so the tissue specific pattern of neurodegeneration in mitochondrial diseases could depend on the molecular profile of mitochondrial pathology and of immunological activation. An induction of *Stat1* mRNA expression and widespread transcriptional activation of the innate immune defense was also observed in ClpP-null mice, fine-tuned to the detection of immunostimulatory nucleic acids particularly via cytosolic sensors and RLR signaling. These downstream pathways were similarly affected by ClpP homozygous deletion as in previous reports about TFAM heterozygous deletion, but more severe than findings in PINK1 and PARKIN mutants. Thus, the cytosolic sensors of DNA and RNA might constitute a general response network to dysfunctions in mitochondria and in the cytosolic translation pathway. For all such disorders, the documentation of their innate immune profile and a neuroprotective trial via STING depletion may be rewarding in the future.

Supplementary Materials: The following are available online at www.mdpi.com/xxx/s1, **Figure S1: Profile of innate immune signaling anomalies regarding mRNA expression and protein abundance levels.**

 doi:10.20944/preprints202105.0021.v1

Author Contributions: In this collaborative study between four departments in two cities, the individual contributions are defined subsequently: Conceptualization, A.M., J.K., I.W., S.G., S.T.-O., A.P.W. and G.A.; methodology, A.M., J.K., I.W., S.G., G.K, J.C.-P., S.T.-O. and A.P.W.; software, A.M., J.K. and I.W.; validation, A.M., J.K., S.G., G.K. and S.T.-O.; formal analysis, A.M., J.K., S.G., S.T.-O.; investigation, I.W., A.P.W. and G.A.; resources, I.W., S.G., A.P.W. and G.A.; data curation, I.W.; writing—original draft preparation, A.M., J.K. and G.A.; writing—review and editing, I.W., S.G., S.T.-O. and A.P.W.; visualization, A.M. and J.K.; supervision, I.W., A.P.W. and G.A.; project administration, G.A.; funding acquisition, I.W., A.P.W. and G.A.. All authors have read and agreed to the published version of the manuscript.

Funding: This research was supported mainly with internal funds of the Goethe University Frankfurt. IW was financed by a grant to the German Network for Mitochondrial Disorders (mitoNET, 01GM1906D), by the Deutsche Forschungsgemeinschaft (DFG) (SFB 815/Z1), and by the Cardio Pulmonary Institute (CPI) of the DFG (EXC2026 and TRR267-Z02. P.W. and S.T-O. were supported by the Office of the Assistant Secretary of Defense for Health Affairs, U.S. Department of Defense Awards W81XWH-17-1-0052 and W81XWH-20-1-0150 (to A.P.W.) through the Peer Reviewed Medical Research Programs. Additional support was provided by National Heart, Lung, and Blood Institute, National Institutes of Health (NIH) Grant R01HL148153 (to A.P.W.). Opinions, interpretations, conclusions, and recommendations are those of the authors and are not necessarily endorsed by the NIH or the U.S. Department of Defense.

Acknowledgments: We are grateful for the help received from the staff at the ZFE animal facility of the Medical Faculty of Frankfurt University. Many thanks to Jana Meisterknecht for excellent technical assistance.

Conflicts of Interest: The authors declare no conflict of interest.

Abbreviations

1	ACTB	β-actin
2	Aim2	Interferon-inducible protein Absent in Melanoma 2, aka PYHIN4
3	aka	also known as
4	ASO	antisense oligonucleotide
5	ATP	adenosine tris-phosphate
6	BAK1	BCL2-antagonist/killer 1, in OMM
7	BAX	BCL2-associated X protein, in OMM
8	BCL2	B cell leukemia/lymphoma 2, apoptosis regulator in OMM
9	BSA	bovine serum albumin
10	cDNA	Complementary deoxy-ribonucleic acid
11	CEB	cytosol extract buffer
12	cGAS	Cyclic GMP-AMP synthase, aka MB21D1
13	ClpB	Caseinolytic mitochondrial matrix peptidase ATP-binding subunit B
14	ClpP	Caseinolytic mitochondrial matrix peptidase proteolytic subunit
15	ClpX	Caseinolytic mitochondrial matrix peptidase AAA ATPase chaperonin
16	DAMP	damage-associated molecular pattern
17	DDX58	DExD/H-box helicase 58, aka RIG-I
18	DMEM	Dulbecco's modified Eagle medium
19	DNA	Deoxyribo-nucleic acid
20	DnaJ	*E. coli* protein J needed for DNA replication, aka Hsp40
21	DNAJA3	DnaJ heat shock protein family (Hsp40) member A3, aka TID1
22	DNAJC30	DnaJ heat shock protein family (Hsp40) member C30
23	DPBS	Dulbecco's phosphate buffered saline
24	dsDNA	double-stranded DNA
25	dsRNA	double-stranded RNA
26	*E. coli*	*Escherichia coli* bacteria
27	EDTA	Ethylenediaminetetraacetic acid
28	EGTA	Ethylene glycol-bis(β-aminoethyl ether)-*N*,*N*,*N*′,*N*′-tetraacetic acid
29	EIF2AK2	Eukaryotic translation initiation factor 2 alpha kinase 2, aka PKR
30	ER	endoplasmic reticulum
31	ERAL1	Era-like 12S mitochondrial rRNA chaperone 1

 doi:10.20944/preprints202105.0021.v1

etc.	etcetera
FBS	Fetal bovine serum
GAPDH	Glyceraldehyde-3-phosphate dehydrogenase
GBP3	Guanylate binding protein 3
GGPS1	geranylgeranyl diphosphate synthase 1
GrpE	*Gro-P* like protein E, in *E. coli* bacteria
GRPEL1	GrpE-like 1, mitochondrial
GTP	guanosine tris-phosphate
GTPBP3	GTP binding protein 3, mitochondrial
HARS2	Histidyl-tRNA synthetase 2, mitochondrial
hrCNE	high-resolution clear native electrophoresis
HSD17B4	Hydroxysteroid 17-beta dehydrogenase 4
Hsp60	Heat shock protein with 60 kiloDalton, aka chaperonin, homolog of GroEL
Hsp70	Heat shock protein with 70 kiloDalton, aka DnaK
HSPA9	Heat shock protein family A (Hsp70) member 9; aka Mortalin
IFI204	Interferon-activated gene 204
Ifi205b	Interferon-activated gene 205b, aka Mnda
Ifi35	Interferon-induced protein 35
IFI44	Interferon-induced protein 44
IFIH1	Interferon-induced with helicase C domain 1, aka MDA-5
IFIT1	Interferon-induced protein with tetratricopeptide repeats 1
IFIT3	Interferon-induced protein with tetratricopeptide repeats 3
IFN-I	Interferon type 1
IFNA1	Interferon alpha 1
IFNAR1	Interferon (alpha and beta) receptor 1
IFNAR2	Interferon (alpha and beta) receptor 2
IFNB1	Interferon beta 1
IκBα	NF-kappa-B inhibitor alpha, aka NFKBIA
IKKα	Inhibitor of nuclear nactor kappa-B kinase subunit alpha, aka CHUK
IKKβ	Inhibitor of nuclear nactor kappa-B kinase subunit beta, aka IKBKB
IL18	Interleukin 18, aka Interferon-gamma-inducing factor
IL1B	Interleukin-1 beta, aka Catabolin
IL6	Interleukin-6, aka Interferon beta 2
IRF3	Interferon regulatory factor 3
IRF7	Interferon regulatory factor 7
ISG15	Interferon-induced 15 kDa protein, ubiquitin-like
ISGs	Interferon-stimulated genes
ISRE	Interferon-stimulated response element
JAK	Janus Kinase
kDa	kiloDalton
LAMIN A/C	nuclear envelope protein LAMIN splice isoforms A and C
LARS2	Leucyl-tRNA synthetase 2, mitochondrial
MAVS	mitochondrial antiviral signaling protein
MEF	Mouse embryonic fibroblasts
MLB	mitochondrial lysis buffer
MNDA	Myeloid nuclear differentiation antigen, aka Interferon-activated gene 205b
MRG	mitochondrial ribosomal granule
mRNA	messenger Ribo-nucleic acid
mtDAMP	mitochondrial Damage-associated molecular pattern
mtDNA	mitochondrial DNA
mtdsRNA	mitochondrial double-stranded RNA
mtRNA	mitochondrial RNA

84	MTRNR1	mitochondrially encoded 12S rRNA
85	NADH	Nicotinamide adenine dinucleotide in its reduced form
86	NDUFB8	NADH:ubiquinone oxidoreductase subunit B8
87	Nfkb1	Nuclear factor of kappa light polypeptide gene enhancer in B cells 1, aka p105
88	NFκB P65	Nuclear factor kappa-B P65 subunit, aka RELA
89	NLR	Nuclear oligomerization-domain like receptor
90	Nlrp3	NLR family, pyrin domain containing 3
91	Nlrx1	NLR family member X1
92	NP-40	Nonyl phenoxypolyethoxylethanol, aka Nonoxynol-40
93	ns	not significant
94	n.s.b.	no specific bands
95	OAS1B	2'-5' Oligoadenylate synthetase 1B
96	OASL2	2'-5' Oligoadenylate synthetase-like 2
97	OMM	outer mitochondrial membrane
98	OXPHOS	oxidative phosphorylation
99	PARKIN	Parkinson juvenile disease protein 2, E3 ubiquitin protein ligase at OMM
100	PCR	Polymerase chain reaction
101	PD	Parkinson's disease
102	PEX6	Peroxisomal biogenesis factor 6
103	PINK1	PTEN-induced kinase 1, protein in OMM
104	PMSF	Phenylmethylsulfonyl fluoride, a serine protease inhibitor
105	PNPT1	Polyribonucleotide nucleotidyltransferase 1
106	POLG	DNA polymerase gamma, catalytic subunit, mitochondrial
107	PORIN-1	mitochondrial outer membrane protein PORIN-1, aka VDAC1
108	PRLTS3	Perrault syndrome type 3
109	PRR	Pattern recognition receptor
110	PTEN	Phosphatase and tensin homolog
111	RIPA	radio-immune-precipitation assay buffer
112	RLR	Retinoic-acid-inducible gene like receptor
113	RMND1	Required for meiotic nuclear division 1 homolog
114	RNA	Ribo-nucleic acid
115	ROS	radical oxygen species
116	rpm	rotations per minute
117	RRM2B	Ribonucleotide reductase regulatory TP53 inducible subunit M2B
118	rRNA	ribosomal Ribo-nucleic acid
119	RSAD2	Radical S-adenosyl methionine domain containing 2
120	RT	Room temperature
121	RT-qPCR	Reverse-transcriptase real-time quantitative polymerase chain reaction
122	*S. cerevisiae*	*Saccharomyces cerevisiae* yeast strain
123	SDS	Sodium dodecyl sulfate
124	SEM	Standard error of the mean
125	ssRNA	single-stranded RNA
126	STAT1	Signal transducer and activator of transcription 1
127	STAT2	Signal transducer and activator of transcription 2
128	STING	Stimulator of interferon response cGAMP interactor 1, aka TMEM173
129	SUPV3L1	Suppressor of var1, 3-like 1 (*S. cerevisiae*)
130	TANK	TRAF family member-associated NF-kappa-B activator
131	TBK1	TANK binding kinase 1
132	Tbp	TATA-box binding protein
133	TBS-T	Tris-buffered saline/Tween 20
134	TFAM	Transcription factor A, mitochondrial
135	TFB1M	Transcription factor B1, mitochondrial

 doi:10.20944/preprints202105.0021.v1

TID1	Tumorous imaginal discs protein Tid56 homolog, aka DNAJA3
TLR	Toll-like receptor
Tlr3	Toll-like receptor 3
Tlr9	Toll-like receptor 9
Tmem173	Transmembrane protein 173, aka STING1
TNF-α	Tumor necrosis factor alpha
TRAF	Tumor necrosis factor receptor associated factor
TRAP1	TNF receptor-associated protein 1, aka mitochondrial HSP75
TRIM25	Tripartite motif-containing 25
Trim30a	Tripartite motif-containing 30A
Trim56	Tripartite motif-containing 56
TRIS	Tris(hydroxymethyl)aminomethane
TRMU	mitochondrial tRNA mitochondrial 2-thiouridylase, aka MTO2
tRNA	transfer Ribo-nucleic acid
Tspan6	Tetraspanin 6
TWNK	Twinkle mtDNA helicase
UPR^{mt}	mitochondrial Unfolded protein response
VDAC	Voltage-dependent anion channel, aka PORIN, in OMM
v/v	volume per volume
WB	Western blot
WT	Wild-Type
ZFE	Central Animal Facility, University Hospital Frankfurt/Main

160

161

162

163 **Supplementary Material**

Preprints (www.preprints.org) | NOT PEER-REVIEWED | Posted: 4 May 2021 doi:10.20944/preprints202105.0021.v1

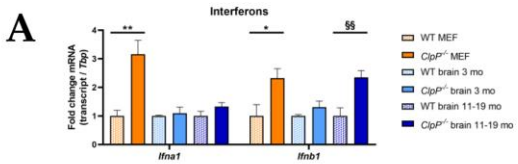

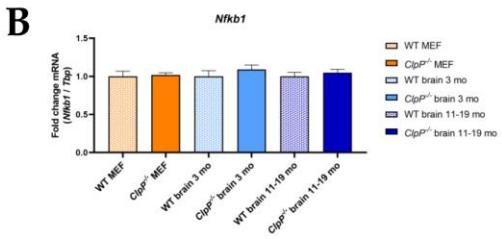

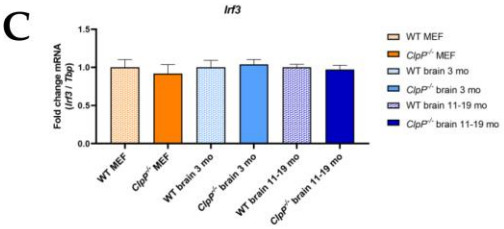

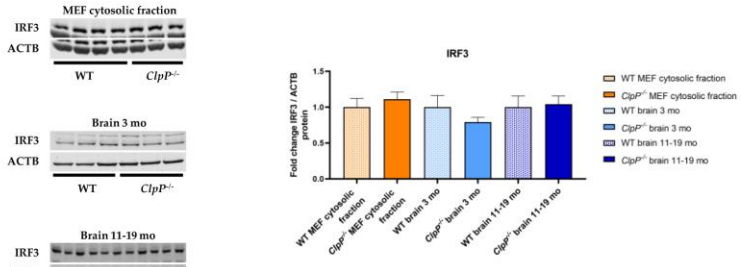

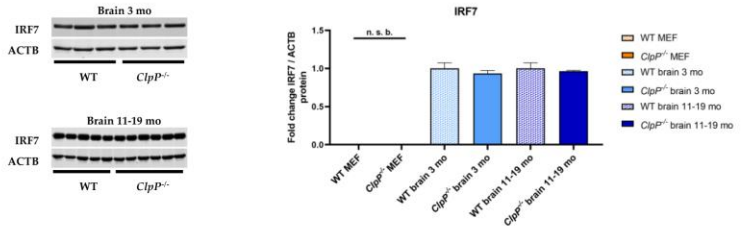

Preprints (www.preprints.org) | NOT PEER-REVIEWED | Posted: 4 May 2021 doi:10.20944/preprints202105.0021.v1

D

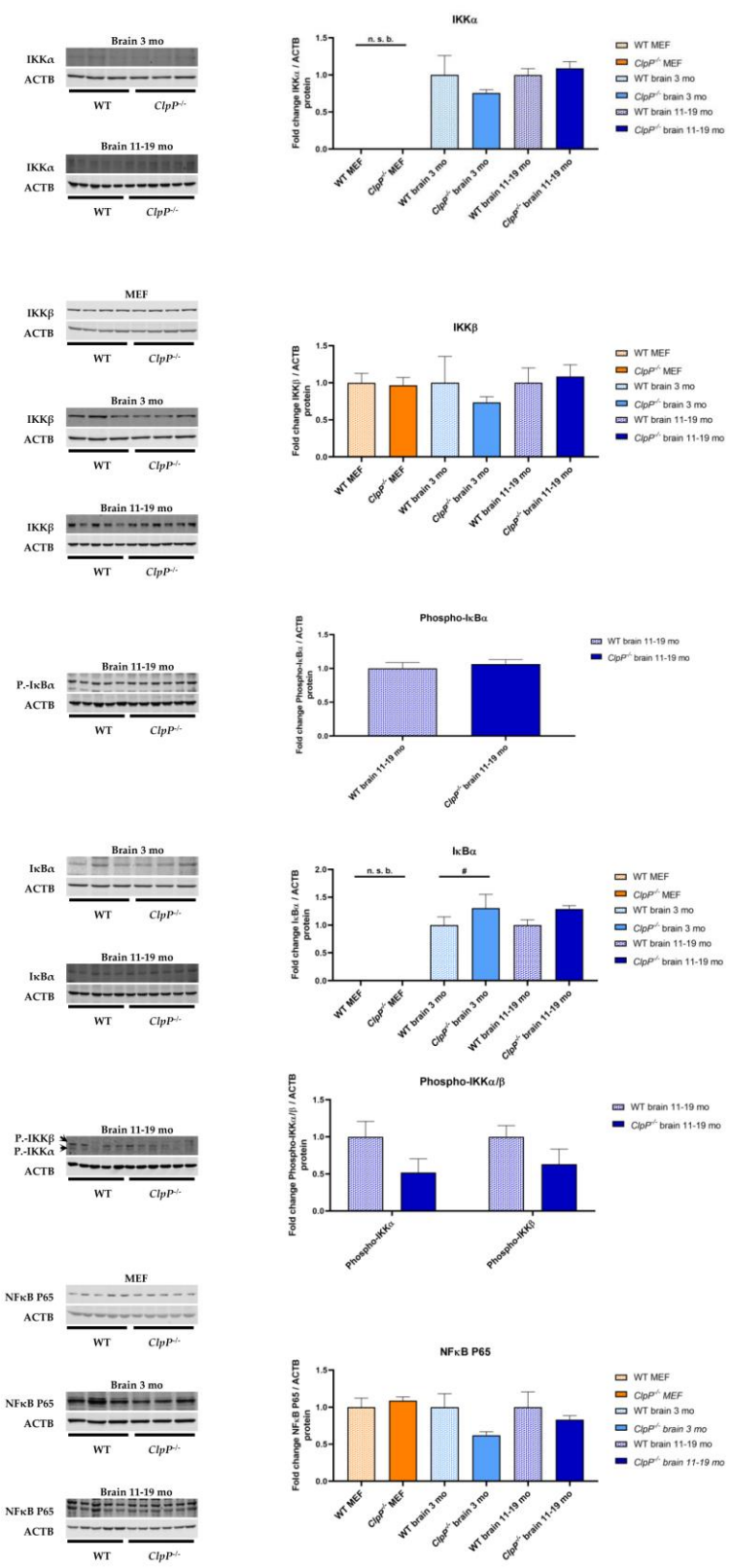

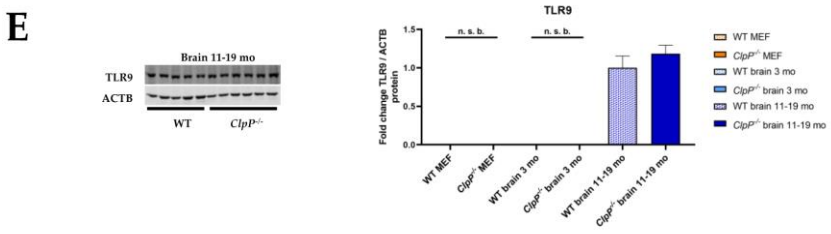

Figure S1. Profile of innate immune signaling anomalies regarding mRNA expression and protein abundance levels. RT-qPCR of **(A)** interferons *Ifna1* and *Ifnb1*, **(B)** analysis of *Nfkb1* mRNA expression via RT-qPCR, **(C)** RT-qPCR of *Irf3* and quantitative immunoblots of IRF3 and IRF7 **(D)** Quantitative immunoblots of NFκB-associated factors, and **(E)** TLR9. Immunoblots were normalized to ACTB, RT-qPCRs to *Tbp*. Data are presented as mean ± SEM. WTs are shown as checked, *ClpP*$^{-/-}$ as plain colored bar graphs. Statistical significances are illustrated by symbols: * or # $p < 0.05$; ** or §§ $p < 0.01$; not significant (ns) $p > 0.05$. Asterisks portray significant differences between WT and *ClpP*$^{-/-}$ MEFs, hashtags show significant effects in brain of 3 month-old WT versus *ClpP*$^{-/-}$ mice, and section signs visualize significant differences in brain of 11-19 month-old WT versus *ClpP*$^{-/-}$ mice. n. s. b.= no specific bands. WT MEF: n= 4-5; *ClpP*$^{-/-}$ MEF: n= 3-5; WT brain 3 months: n= 2-3; *ClpP*$^{-/-}$ brain 3 months: n= 3; WT brain 11-19 months: n= 4-5; *ClpP*$^{-/-}$ brain 11-19 months: n= *4-6*.

References

1. Jenkinson, E.M., et al., *Perrault syndrome is caused by recessive mutations in CLPP, encoding a mitochondrial ATP-dependent chambered protease.* American journal of human genetics, 2013. **92**(4): p. 605–613.
2. Newman, W.G., et al., *GeneReviews®: Perrault Syndrome*. 1993: Seattle (WA).
3. Bhaskaran, S., et al., *Loss of mitochondrial protease ClpP protects mice from diet-induced obesity and insulin resistance.* EMBO reports, 2018. **19**(3).
4. Nishi, Y., et al., *The Perrault syndrome: clinical report and review.* American journal of medical genetics, 1988. **31**(3): p. 623–629.
5. Theunissen, T.E.J., et al., *Specific MRI Abnormalities Reveal Severe Perrault Syndrome due to CLPP Defects.* Frontiers in neurology, 2016. **7**: p. 203.
6. Sherman, M.Y. and A.L. Goldberg, *Involvement of molecular chaperones in intracellular protein breakdown.* EXS, 1996. **77**: p. 57-78.
7. Haynes, C.M., et al., *ClpP mediates activation of a mitochondrial unfolded protein response in C. elegans.* Developmental cell, 2007. **13**(4): p. 467–480.
8. Szczepanowska, K., et al., *CLPP coordinates mitoribosomal assembly through the regulation of ERAL1 levels.* The EMBO journal, 2016. **35**(23): p. 2566–2583.
9. Torres-Odio, S., et al., *Loss of Mitochondrial Protease CLPP Activates Type I IFN Responses through the Mitochondrial DNA-cGAS-STING Signaling Axis.* Journal of immunology (Baltimore, Md. : 1950), 2021.
10. Gispert, S., et al., *Loss of mitochondrial peptidase Clpp leads to infertility, hearing loss plus growth retardation via accumulation of CLPX, mtDNA and inflammatory factors.* Human molecular genetics, 2013. **22**(24): p. 4871–4887.

11. Key, J., et al., *Loss of mitochondrial ClpP, Lonp1, and Tfam triggers transcriptional induction of Rnf213, a susceptibility factor for moyamoya disease.* Neurogenetics, 2020. **21**(3): p. 187–203.
12. Oziębło, D., et al., *Two Novel Pathogenic Variants Confirm RMND1 Causative Role in Perrault Syndrome with Renal Involvement.* Genes, 2020. **11**(9).
13. Tucker, E.J., et al., *Genomic sequencing highlights the diverse molecular causes of Perrault syndrome: a peroxisomal disorder (PEX6), metabolic disorders (CLPP, GGPS1), and mtDNA maintenance/translation disorders (LARS2, TFAM).* Human genetics, 2020. **139**(10): p. 1325–1343.
14. Rauthan, M., et al., *The mitochondrial unfolded protein response activator ATFS-1 protects cells from inhibition of the mevalonate pathway.* Proceedings of the National Academy of Sciences of the United States of America, 2013. **110**(15): p. 5981–5986.
15. Raimundo, N., et al., *Mitochondrial stress engages E2F1 apoptotic signaling to cause deafness.* Cell, 2012. **148**(4): p. 716–726.
16. Hutchin, T.P. and G.A. Cortopassi, *Mitochondrial defects and hearing loss.* Cellular and molecular life sciences : CMLS, 2000. **57**(13-14): p. 1927–1937.
17. Greber, B.J., et al., *Ribosome. The complete structure of the 55S mammalian mitochondrial ribosome.* Science (New York, N.Y.), 2015. **348**(6232): p. 303–308.
18. West, A.P., G.S. Shadel, and S. Ghosh, *Mitochondria in innate immune responses.* Nature reviews. Immunology, 2011. **11**(6): p. 389–402.
19. West, A.P., et al., *Mitochondrial DNA stress primes the antiviral innate immune response.* Nature, 2015. **520**(7548): p. 553–557.
20. Andreeva, L., et al., *cGAS senses long and HMGB/TFAM-bound U-turn DNA by forming protein-DNA ladders.* Nature, 2017. **549**(7672): p. 394–398.
21. Wu, Z., et al., *Mitochondrial DNA Stress Signalling Protects the Nuclear Genome.* Nature metabolism, 2019. **1**(12): p. 1209–1218.
22. Zhang, W., et al., *Cellular DNAJA3, a Novel VP1-Interacting Protein, Inhibits Foot-and-Mouth Disease Virus Replication by Inducing Lysosomal Degradation of VP1 and Attenuating Its Antagonistic Role in the Beta Interferon Signaling Pathway.* Journal of virology, 2019. **93**(13).
23. West, A.P. and G.S. Shadel, *Mitochondrial DNA in innate immune responses and inflammatory pathology.* Nature reviews. Immunology, 2017. **17**(6): p. 363–375.
24. Dhir, A., et al., *Mitochondrial double-stranded RNA triggers antiviral signalling in humans.* Nature, 2018. **560**(7717): p. 238–242.
25. Corti, O., S. Lesage, and A. Brice, *What genetics tells us about the causes and mechanisms of Parkinson's disease.* Physiological reviews, 2011. **91**(4): p. 1161–1218.
26. Pickrell, A.M. and R.J. Youle, *The roles of PINK1, parkin, and mitochondrial fidelity in Parkinson's disease.* Neuron, 2015. **85**(2): p. 257–273.
27. Manzanillo, P.S., et al., *The ubiquitin ligase parkin mediates resistance to intracellular pathogens.* Nature, 2013. **501**(7468): p. 512–516.
28. Torres-Odio, S., et al., *Progression of pathology in PINK1-deficient mouse brain from splicing via ubiquitination, ER stress, and mitophagy changes to neuroinflammation.* Journal of neuroinflammation, 2017. **14**(1): p. 154.
29. Sliter, D.A., et al., *Parkin and PINK1 mitigate STING-induced inflammation.* Nature, 2018. **561**(7722): p. 258–262.

30. Crooks, D.R., et al., *Mitochondrial DNA alterations underlie an irreversible shift to aerobic glycolysis in fumarate hydratase-deficient renal cancer.* Science signaling, 2021. **14**(664).
31. Ryan, D.G., et al., *Coupling Krebs cycle metabolites to signalling in immunity and cancer.* Nature metabolism, 2019. **1**: p. 16–33.
32. Krysko, D.V., et al., *Emerging role of damage-associated molecular patterns derived from mitochondria in inflammation.* Trends in immunology, 2011. **32**(4): p. 157–164.
33. Larsson, N.G., et al., *Down-regulation of mitochondrial transcription factor A during spermatogenesis in humans.* Human molecular genetics, 1997. **6**(2): p. 185–191.
34. Lee, E.J., et al., *Negative transcriptional regulation of mitochondrial transcription factor A (TFAM) by nuclear TFAM.* Biochemical and biophysical research communications, 2014. **450**(1): p. 166–171.
35. Meier, J.A. and A.C. Larner, *Toward a new STATe: the role of STATs in mitochondrial function.* Seminars in immunology, 2014. **26**(1): p. 20–28.
36. Sehgal, P.B., *Plasma membrane rafts and chaperones in cytokine/STAT signaling.* Acta biochimica Polonica, 2003. **50**(3): p. 583–594.
37. Lu, B., et al., *Tid1 isoforms are mitochondrial DnaJ-like chaperones with unique carboxyl termini that determine cytosolic fate.* The Journal of biological chemistry, 2006. **281**(19): p. 13150–13158.
38. Beck, J.S., E.J. Mufson, and S.E. Counts, *Evidence for Mitochondrial UPR Gene Activation in Familial and Sporadic Alzheimer's Disease.* Current Alzheimer research, 2016. **13**(6): p. 610–614.
39. Wittig, I., H.P. Braun, and H. Schagger, *Blue native PAGE.* Nat Protoc, 2006. **1**(1): p. 418-28.
40. Wittig, I., M. Karas, and H. Schagger, *High resolution clear native electrophoresis for in-gel functional assays and fluorescence studies of membrane protein complexes.* Mol Cell Proteomics, 2007. **6**(7): p. 1215-25.
41. Schmittgen, T.D. and K.J. Livak, *Analyzing real-time PCR data by the comparative C(T) method.* Nat Protoc, 2008. **3**(6): p. 1101-8.
42. Sen, N.-E., et al., *Generation of an Atxn2-CAG100 knock-in mouse reveals N-acetylaspartate production deficit due to early Nat8l dysregulation.* Neurobiology of disease, 2019. **132**: p. 104559.
43. Yochem, J., et al., *Genetic analysis of two genes, dnaJ and dnaK, necessary for Escherichia coli and bacteriophage lambda DNA replication.* Mol Gen Genet, 1978. **164**(1): p. 9-14.
44. Copeland, E., et al., *hTID-1 defines a novel regulator of c-Met Receptor signaling in renal cell carcinomas.* Oncogene, 2011. **30**(19): p. 2252-63.
45. Cheng, H., et al., *Molecular mechanism of hTid-1, the human homolog of Drosophila tumor suppressor l(2)Tid, in the regulation of NF-kappaB activity and suppression of tumor growth.* Mol Cell Biol, 2005. **25**(1): p. 44-59.
46. Kim, S.W., et al., *Tid1 negatively regulates the migratory potential of cancer cells by inhibiting the production of interleukin-8.* Cancer Res, 2005. **65**(19): p. 8784-91.
47. Kumada, K., et al., *HSP70/DNAJA3 chaperone/cochaperone regulates NF-kappaB activity in immune responses.* Biochem Biophys Res Commun, 2019. **513**(4): p. 947-951.
48. Konieczny, I. and M. Zylicz, *Role of bacterial chaperones in DNA replication.* Genet Eng (N Y), 1999. **21**: p. 95-111.

49. Seo, G.J., et al., *TRIM56-mediated monoubiquitination of cGAS for cytosolic DNA sensing.* Nature communications, 2018. **9**(1): p. 613.
50. Fredriksson, A., et al., *Decline in ribosomal fidelity contributes to the accumulation and stabilization of the master stress response regulator sigmaS upon carbon starvation.* Genes Dev, 2007. **21**(7): p. 862-74.
51. Becker, L.A., et al., *Therapeutic reduction of ataxin-2 extends lifespan and reduces pathology in TDP-43 mice.* Nature, 2017. **544**(7650): p. 367-371.
52. Mercuri, E., et al., *Nusinersen versus Sham Control in Later-Onset Spinal Muscular Atrophy.* N Engl J Med, 2018. **378**(7): p. 625-635.
53. Antonellis, A. and E.D. Green, *The role of aminoacyl-tRNA synthetases in genetic diseases.* Annu Rev Genomics Hum Genet, 2008. **9**: p. 87-107.
54. Kokotas, H., M.B. Petersen, and P.J. Willems, *Mitochondrial deafness.* Clin Genet, 2007. **71**(5): p. 379-91.
55. Demain, L.A., G.S. Conway, and W.G. Newman, *Genetics of mitochondrial dysfunction and infertility.* Clin Genet, 2017. **91**(2): p. 199-207.
56. Ognjenovic, J. and M. Simonovic, *Human aminoacyl-tRNA synthetases in diseases of the nervous system.* RNA Biol, 2018. **15**(4-5): p. 623-634.
57. Opinc, A.H. and J.S. Makowska, *Antisynthetase syndrome - much more than just a myopathy.* Semin Arthritis Rheum, 2021. **51**(1): p. 72-83.
58. Adang, L., et al., *Developmental Outcomes of Aicardi Goutieres Syndrome.* J Child Neurol, 2020. **35**(1): p. 7-16.
59. Bamborschke, D., et al., *PNPT1 mutations may cause Aicardi-Goutieres-Syndrome.* Brain Dev, 2021. **43**(2): p. 320-324.
60. Stenton, S.L., et al., *Impaired complex I repair causes recessive Leber's hereditary optic neuropathy.* J Clin Invest, 2021. **131**(6).